HNPS Advances in Nuclear Physics

Vol 28 (2021)

HNPS2021

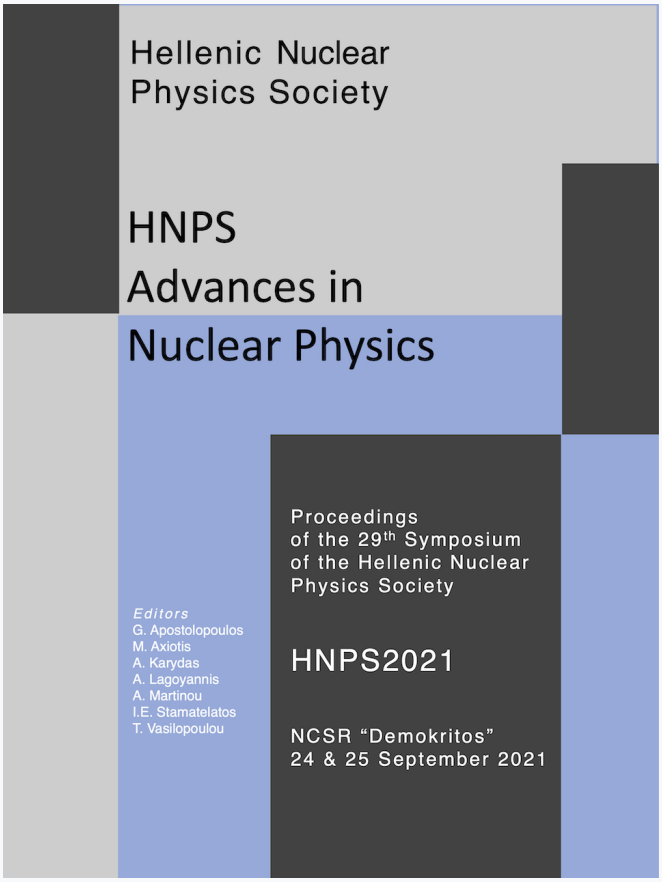

A study of shape transition and bubbleness in Ne isotopes

Pankaj Kumar, Virender Thakur, Shashi K. Dhiman

doi: 10.12681/hnps.3540

A study of shape transition and bubbleness in Ne isotopes

Pankaj Kumar[1,*], Virender Thakur[1], Shashi K. Dhiman[1]

[1] *Department of Physics, Himachal Pradesh University, Summerhill, Shimla-171005, India*

Abstract We have studied shape transition and development of quadrupole deformation in even-even $^{18\text{-}36}$Ne isotopes by employing covariant density functional theory (CDFT) with density-dependent meson exchange (DD-ME2) and density-dependent point coupling (DD-PC1) parameter sets. A sudden shape transition is observed in the Ne isotopic chain and can be related to the evolution of shell structure of single-particle orbitals. The correlations between shape transition and discontinuities in other physical observables are also examined. Our results for ground-state properties are in good agreement with the available experimental data and the result of various theoretical models. The present calculations infer the neutron drip line at ^{34}Ne. In addition to shape transition, the bubble structure is also studied for magic nuclei in this chain.

Keywords Covariant density functional, Shape coexistence, Charge radii, Bubble structure

INTRODUCTION

The development of accelerator techniques and sensitive detection technologies for Radioactive Ion Beams provide the possibility of studying the structural properties of nuclei away from the stability line. The nuclei in the light-mass region are of particular interest. These nuclei are at the center of the island of inversion. The evolution of nuclear shapes in various isotopic and isotonic chains has been investigated consistently by various theoretical and experimental techniques. The phenomena of shape coexistence and triaxial deformation were studied for some light nuclei [1,2]. However, the effect of triaxiality was found to be marginal on the mean-field part of binding energy. A halo structure of ^{31}Ne was reported experimentally using one proton removal reaction [3]. A recent experimental investigation suggests ^{34}Ne as the heaviest bound nucleus in Ne isotopic chain [4]. In a recent study, the N = 14 sub-shell closure was reported for charge radii measurement of neon isotopes. Their computations were based on nucleon-nucleon and three-nucleon potentials from chiral effective field theory [5].

Nuclear density functional theories (DFT) have been used to understand nuclear many-body dynamics for an appreciable description of nuclei near the drip line. Covariant density functional theory (CDFT) is one of the most attractive nuclear density functional theories and has achieved great success in the description of ground- and excited-state properties of both spherical and deformed nuclei throughout the nuclear chart [6-9]. In this work, a systematic study of shape transition and ground state properties of neon isotopes has been done using CDFT with DD-ME2 [10] and DD-PC1 [11] parameter sets with a separable pairing interaction [12,13]. The calculations were performed within an axially symmetric deformed configuration.

THEORETICAL FRAMEWORK

Self-consistent mean-field (SCMF) models provide a very successful tool to study a variety of nuclear structure phenomena throughout the segre chart. These models are based on nuclear energy

* Corresponding author, email: pankajdhiman659@gmail.com

density functionals in which the nucleons are treated as independent particles moving inside the nucleus under the potentials derived from such functionals [14].

Meson exchange models

In relativistic case, the nucleons are treated as four component Dirac spinors interacting via the exchange of virtual mesons. The Lagrangian density for meson-exchange model is given by [10]

$$\mathcal{L} = \sum_i \overline{\psi_i}\left(i\gamma_\mu \partial^\mu - m\right)\psi_i - \frac{1}{2}\partial_\mu \sigma \partial^\mu \sigma - \frac{1}{2}m_\sigma^2\sigma^2 - \frac{1}{2}\Omega_{\mu\nu}\Omega^{\mu\nu} + \frac{1}{2}m_\omega^2\omega_\mu\omega^\mu - \frac{1}{4}\boldsymbol{R}_{\mu\nu}\boldsymbol{R}^{\mu\nu}$$
$$+\frac{1}{2}m_\rho^2\overrightarrow{\rho_\mu}.\overrightarrow{\rho^\mu} - \frac{1}{4}\boldsymbol{F}_{\mu\nu}\boldsymbol{F}^{\mu\nu} - g_\sigma\bar{\psi}\psi\sigma - g_\omega\bar{\psi}\gamma^\mu\psi\omega_\mu - g_\rho\bar{\psi}\vec{\tau}\gamma^\mu\psi.\overrightarrow{\rho_\mu} - e\bar{\psi}\gamma^\mu\psi\boldsymbol{A}_\mu, \quad (1)$$

where the first term represents the Lagrangian for free nucleons with bare mass *m* and ψ denotes the Dirac spinor. $m_\sigma, m_\omega, m_\rho$ are the masses of σ, ω, ρ mesons with the corresponding coupling constants g_σ, g_ω, and g_ρ for the mesons to the nucleons. $\Omega_{\mu\nu}, \boldsymbol{R}_{\mu\nu}, \boldsymbol{F}_{\mu\nu}$ are field tensor for vector fields $\omega, \rho,$ and the photon.

The functionals are described by density-dependent coupling constants $g_i(\rho)$. The coupling of σ and ω fields to the nucleon field reads [15]

$$g_i = g_i(\rho_{sat})f_i(x) \qquad \text{for } i = \sigma, \omega \quad (2)$$

with

$$f_i(x) = a_i\frac{1+b_i(x+d_i)^2}{1+c_i(x+d_i)^2} \quad (3)$$

here, $x = \rho/\rho_{sat}$. The ρ_{sat} is the baryon density at saturation in symmetric nuclear matter whose value is taken as $0.152\ fm^{-3}$ in present models.

For density dependence of ρ meson coupling, the functional form is given by [16]

$$g_\rho(\rho) = g_\rho(\rho_{sat})e^{-a_\rho(x-1)} \quad (4)$$

The isovctor channel is parameterized by $g_\rho(\rho)$ and a_ρ. This model is represented by the parameter set DD-ME2 [10].

Point coupling models

The Lagrangian density of the point coupling model includes the isoscalar-scaler, isoscalar-vector and isovector-vector four-fermion contact interactions in the isospace-space and have form[11]:

$$\mathcal{L} = \bar{\psi}(i\gamma.\partial - m)\psi - \frac{1}{2}\alpha_S(\rho)(\bar{\psi}\psi)(\bar{\psi}\psi) - \frac{1}{2}\alpha_V(\rho)(\bar{\psi}\gamma^\mu\psi)(\bar{\psi}\gamma_\mu\psi) - \frac{1}{2}\alpha_{TV}(\rho)(\bar{\psi}\tau\gamma^\mu\psi)$$
$$(\bar{\psi}\tau\gamma_\mu\psi) - \frac{1}{2}\delta_S(\partial_\nu\bar{\psi}\psi)(\partial^\nu\bar{\psi}\psi) - e\bar{\psi}\gamma.\boldsymbol{A}\frac{1-\tau_3}{2}\psi, \quad (5)$$

In addition to free nucleon Lagrangian and the point coupling interaction terms, the above Lagrangian density also includes the coupling of protons to the electromagnetic field. The derivative term in the above equation accounts for the effects of finite-range interactions.

The functional form of couplings is given by

$$\alpha_i(\rho) = a_i + (b_i + c_i x)e^{-d_i x} \qquad (i = S, V, TV) \tag{6}$$

Covariant density functional theory with separable pairing interaction

It is important to incorporate pairing correlations for a quantitative description of open-shell nuclei [12,13]. The formulation of RHB model is a relativistic extension of the HFB model in which mean-field and pairing correlations are treated self consistently. The relativistic Hartree-Bogoliubov energy density functional is given by

$$E_{RHB}[\hat{\rho}, \hat{\kappa}] = E_{RMF}[\hat{\rho}] + E_{pair}[\hat{\kappa}] \tag{7}$$

where $E_{RMF}[\hat{\rho}]$ is the nuclear energy density functional and is given by

$$E_{RMF}[\psi, \bar{\psi}, \boldsymbol{A}_\mu] = \int d^3r\, \boldsymbol{\mathcal{H}}(r) \tag{8}$$

The pairing part of RHB functional is given as

$$E_{pair}[\hat{\kappa}] = \frac{1}{4}\sum_{n_1 n_1'} \sum_{n_2 n_2'} \kappa^*_{n_1 n_1'} \langle n_1 n_1' | V^{PP} | n_2 n_2' \rangle \kappa_{n_2 n_2'} \tag{9}$$

where $\langle n_1 n_1' | V^{PP} | n_2 n_2' \rangle$ are the matrix elements of the two-body pairing interaction.
The pairing force is separable in momentum space and in r-space has the form of

$$V^{PP}(\boldsymbol{r_1}, \boldsymbol{r_2}, \boldsymbol{r_1'}, \boldsymbol{r_2'}) = -G\delta(\boldsymbol{R} - \boldsymbol{R'})P(\boldsymbol{r})P(\boldsymbol{r'}) \tag{10}$$

where $\boldsymbol{R} = \frac{1}{\sqrt{2}}(\boldsymbol{r_1} + \boldsymbol{r_2})$ and $\boldsymbol{r} = \frac{1}{\sqrt{2}}(\boldsymbol{r_1} - \boldsymbol{r_2})$ represent the center of mass and the relative coordinates, respectively. The form factor $P(\boldsymbol{r})$ is of Gaussian shape

$$P(\boldsymbol{r}) = \frac{1}{(4\pi a^2)^{3/2}} e^{-r^2/2a^2} \tag{11}$$

The two parameters 'G' and 'a' have been adjusted to reproduce the density dependence of the gap at the Fermi surface for infinite nuclear matter. The pairing force has a finite range and it conserves translational invariance due to the presence of the factor $\delta(\boldsymbol{R} - \boldsymbol{R'})$. Finally, the pairing energy in the nuclear ground state is given by

$$E_{pair} = -G \sum_N P_N^* P_N \tag{12}$$

The total energy for the nuclear system with *A* nucleons can be calculated as [17]

$$E_{tot} = E_{RMF} + E_{pair} + E_{cm} \tag{13}$$

Here, $E_{cm} = \frac{-\langle P^2 \rangle}{2Am}$ accounts for the center-of-mass correction, where $\langle P \rangle = \sum_i^A p_i$ is the total momentum of the nucleus in center of mass frame with *A* nucleons [18].

RESULTS AND DISCUSSION

Shape Transition and quardrupole deformation in Ne isotopes

Atomic nuclei display a variety of geometrical shapes arising from the collective motion of the nucleons [19]. The quadrupole deformation parameter reflects the shape of a nucleus. In axially symmetric case, the deformed nuclei can be classified according to the value of the quadrupole deformation parameter (β_2). A positive value of β_2 corresponds to the prolate shape, and the negative value of β_2 reflects oblate shape nuclei while $\beta_2 = 0$ corresponds to a spherical shape.

Fig. 1 presents the potential energy curves (PECs) for even-even $^{18\text{-}36}$Ne isotopes. The energies are normalized with respect to the total energy of the global minima. The potential energy curve for ^{18}Ne displays a spherical minimum which is expected due to the presence of N = 8 shell closure. Deformed shapes are observed between the shell closures. A large prolate deformation is observed as

one moves from ^{18}Ne to ^{20}Ne. This sudden shape transition can be related to the evolution of the shell structure of single-particle orbitals. The partial filling of single-particle orbitals by excitation of nucleons to higher orbitals favors the onset of deformation. An oblate-prolate shape coexistence can be observed in ^{24}Ne. The nuclei ^{26,28}Ne show shallow minima. The spherical shape is restored when approaching N = 20 shell closure (for ^{30}Ne). When moving away from ^{30}Ne, the shape becomes prolate and remains prolate up to ^{36}Ne.

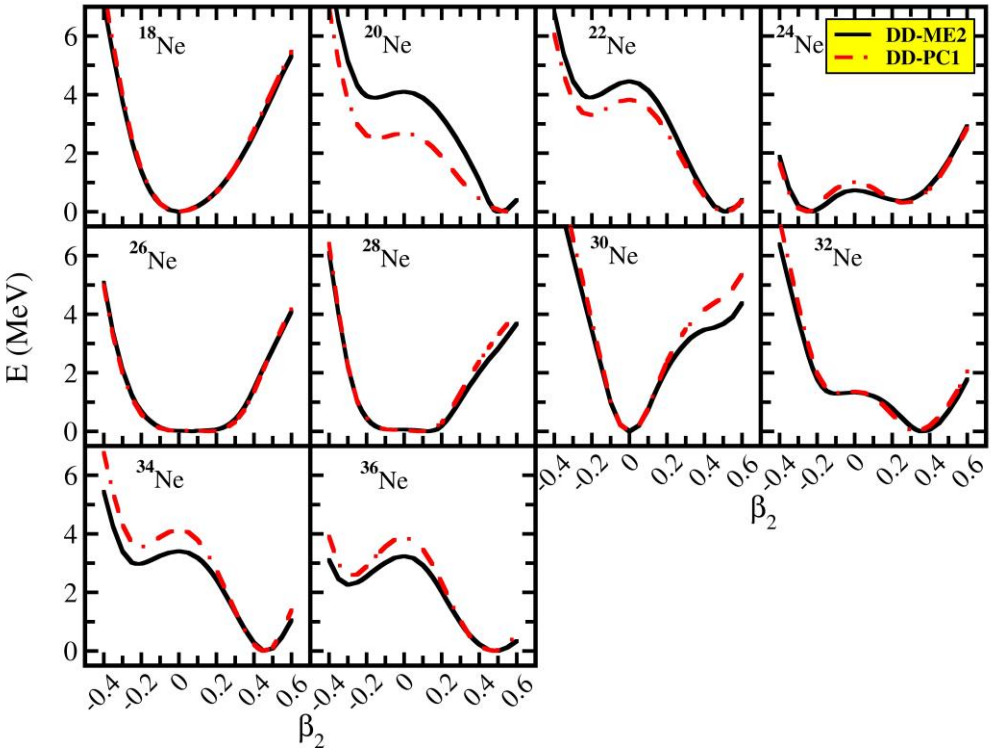

Fig. 1. *The potential energy curves (PECs) for $^{18\text{-}36}$Ne isotopes calculated using CDFT with DD-ME2 and DD PC1 interactions. The energies are normalized with respect to the binding energy of the absolute minima.*

Fig. 2 displays the isotopic evolution of quadrupole deformation parameter β_2 associated with the various minima shown in Fig. 1. From this figure, the progress of deformations with the number of neutrons is more apparent. The calculated values of quadrupole deformation parameter are compared with the results of the finite range droplet model (FRDM) [20] and the HFB model based on the D1S-Gogny force [21]. A good agreement can be observed between the calculated results and the results of other theoretical models.

Two neutron separation energy

The quantity that is related to the stability of a nucleus is two-neutron separation energy, S_{2n}, defined as

$$S_{2n} = E_b(Z,N) - E_b(Z,N-2)$$

This quantity provides information on the stability of a nucleus against the emission of two neutrons and thus defines the neutron drip line. The systematics of S_{2n} are generally known to

decrease with neutron number. This decline in S_{2n} is smooth except at the magic number, where a sharp change in the slope of S_{2n} is observed due to the presence of neutron shell closures.

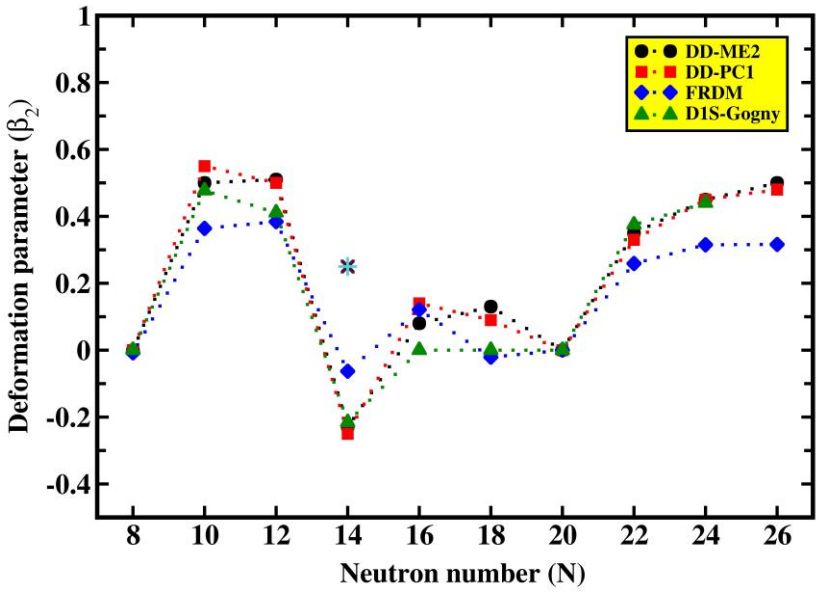

Fig. 2. *The evolution of quadrupole deformation parameter (β_2) as a function of neutron number. The comparison is made with finite range droplet model [20] and HFB model [21].*

Fig. 3 presents the trend of two-neutron separation energy as a function of neutron number. The theoretical results, calculated using DD-ME2 and DD-PC1 interactions, are compared with available experimental data [22]. A sharp decline of S_{2n} at N = 8 and N = 20 supports the existence of shell closures. S_{2n} is an important quantity to predict neutron drip line. A negative value of two-neutron separation energy corresponds to an unbound system [23]. In the present work, the neutron drip line has been observed for ^{34}Ne. Our prediction for the neutron drip line in Ne isotopic chain is consistent with some recent investigations [4,5].

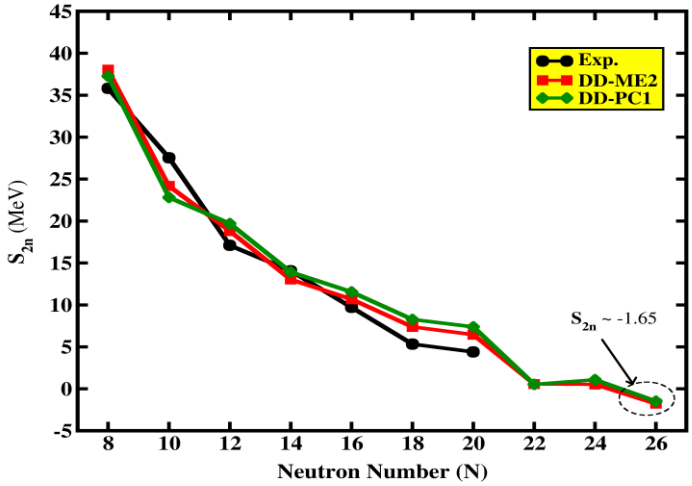

Fig. 3. *Two-neutron separation energy S_{2n} for Ne isotopes, calculated using DD-ME2 and DD-PC1 parameter sets. Comparison is made with available experimental data [22].*

Root-mean-square charge radius

The charge radii are considered among the most sensitive observables to explore the various nuclear structure phenomena such as halo structure [24], shape transition [25], shape coexistence [26], occurrence of magic numbers [27,28], etc. Sudden changes in the behavior of charge radii indicate nuclear shape transitions. In the present work, the rms charge radii are calculated by using the expression $R_{ch} = \sqrt{R_p^2 + 0.64}\ (fm)$, where R_p denotes the rms radius of the proton density distribution and the factor 0.64 included in the equation is a correction due to the finite size of the proton.

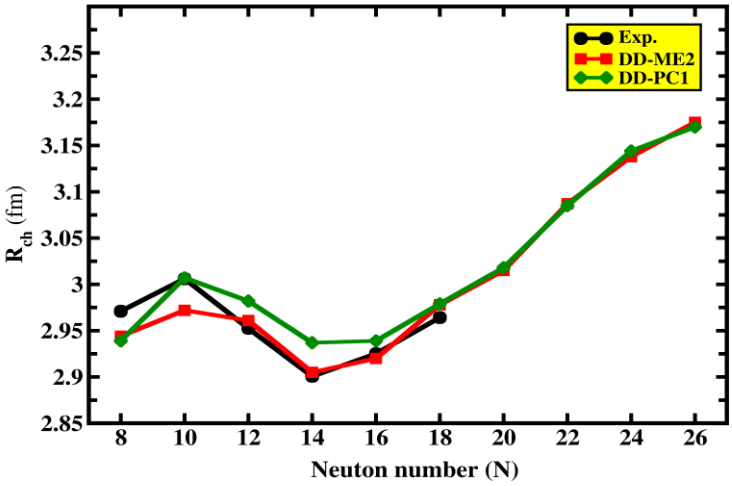

Fig. 4. *Nuclear charge radii for Ne isotopes, calculated using DD-ME2 and DD-PC1 parameter sets. The experimental data are denoted by black filled circles [29].*

Fig. 4 shows the rms charge radii for Ne isotopes calculated using DD-ME2 and DD-PC1 parameter sets. The kink appearing after crossing N = 8 and N = 20 suggest the presence of neutron shell closures. Magic number refers to completely filled shells and hence resulting in a relatively small charge radius. Considering this point, a small value of charge radius for ^{24}Ne indicates the presence of sub-shell closure at N = 14, which is consistent with the data. However, no such sub-shell closure is observed in the trend of two neutron separation energy.

Bubble structure in magic Ne isotopes

The 'Bubble' structure is characterized by the depletion of nucleonic density at the center of the nucleus. The degree of central depletion in proton or neutron densities can be quantified in terms of depletion fraction (DF) defined as

$$DF = \frac{\rho_{max} - \rho_{cen}}{\rho_{max}} \text{ X } 100\%,$$

where ρ_{max} and ρ_{cen} represent the values of maximum and central neutron (or proton) density, respectively.

Panel 'a' and 'b' of Fig. 5 present the neutron and proton density distribution for ^{18}Ne and ^{30}Ne. A clear bubble can be seen in the proton density profiles of these nuclei. ^{18}Ne also shows the bubble structure in neutron density profile.

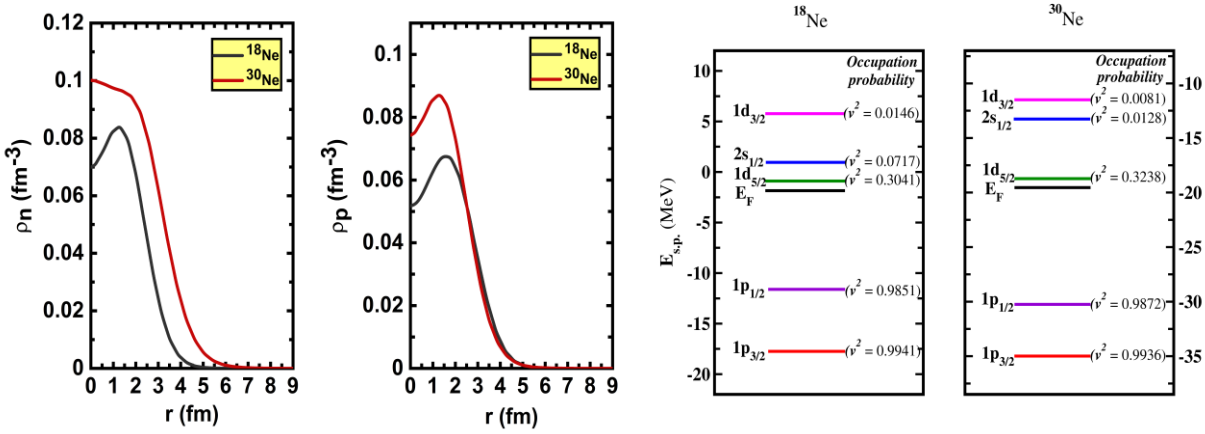

Fig. 5. *(a) Neutron and (b) proton density distributions for ^{18}Ne and ^{30}Ne. (c) Proton single-particle energy levels for ^{18}Ne and for (d) ^{30}Ne. The occupation probabilities are shown in parentheses.*

The formation of bubble structure can be related to the depopulation of the *s*-state, which generally contributes to the nuclear density at the center. Panel 'c' and 'd' of Fig. 5 show the proton single-particle energy levels for ^{18}Ne and ^{30}Ne. The corresponding occupation probabilities for each state are given in parentheses. It can be observed from panel 'c' of Fig. 5 that the $2s_{1/2}$ orbit has low occupation probability resulting in a proton bubble in ^{18}Ne with DF ≈ 16%. However, by increasing in number of neutrons the p-n interaction increases in ^{30}Ne and the $2s_{1/2}$ orbit shifts near the $1d_{3/2}$ orbital resulting in the decrease of the occupation probability and hence the increase in the depletion fraction (DF ≈ 23%).

CONCLUSIONS

In the present work, we have done a systematic study of shape transition and ground state observables in even-even $^{18\text{-}36}$Ne isotopes by employing covariant density functional theory with meson exchange DD-ME2 and point coupling DD-PC1 interactions. A sudden change in the shape is observed in the neon isotopic chain. Most of the isotopes are found to have a prolate ground state. The trend of two-neutron separation energy supports the existence of robust shell closure at N = 8 and N = 20. The negative value of S_{2n} for ^{36}Ne indicate that the heaviest bound nuclei, in the neon isotopic chain, is ^{34}Ne. Our prediction for the neutron drip line is consistent with some recent observations. The systematic of charge radii are in good agreement with available experimental data. The kink appearing after crossing N = 8 and N = 20 indicate the presence of neutron shell closures. In the present study, the charge radii suggest a sub-shell closure at N = 14 but neither theory nor data support this sub-shell closure for the two-neutron separation energies. In addition to these structural changes, a bubble structure has been observed for ^{18}Ne and ^{30}Ne nuclei. The central depletion of density could be related to the depopulation of the $2s_{1/2}$ orbital. The overall results of the ground-state properties Ne isotopic mass chain are in good agreement with the available experimental data and with results obtained from different models.

References

[1] A.D. Davies et al., Phys. Rev. Lett. 96, p. 112503 (2006)

[2] Y. Wang et al., Prog. Theor. Exp. Phys. 2014, p. 113D03 (2014)
[3] T. Nakamura et al., Phys. Rev. Lett. 103, p. 262501 (2009)
[4] DeukSoon Ahn et al., Phys. Rev. Lett. 123, p. 212501 (2019)
[5] S.J. Novario et al., Phys. Rev. C 102, p. 051303 (2020)
[6] V. Thakur et al., Nucl. Phys. A 1002, p. 121981 (2020)
[7] P. Kumar and S.K. Dhiman, Nucl. Phys. A 1001, p. 121935 (2020)
[8] P. Kumar et al., Acta Phys. Pol. B 52, p. 401 (2021)
[9] P. Kumar et al., Eur. Phys. J. A 57, p. 36 (2021)
[10] G.A Lalazissis et al., Phys. Rev. C 71, p. 024312 (2005)
[11] T. Niksic et al., Phys. Rev. C 78, p. 034318 (2008)
[12] Y. Tian et al., Phys. Lett. B 676, p. 44 (2009)
[13] Y. Tian et al., Phys. Rev. C 79, p. 064301 (2009)
[14] M. Bender et al., Rev. Mod. Phys. 75, p. 121 (2003)
[15] S. Typel and H.H. Wolter, Nucl. Phys. A 656, p. 331 (1999)
[16] F. De Jong and H. Lenske, Phys. Rev. C 57, p. 3099 (1998)
[17] P.G. Reinhard, Rep. Prog. Phys. 52, p. 439 (1989)
[18] Zhao Peng-Wei et al., Chin. Rev. Lett. 26, p. 112102 (2009)
[19] A. Bohr and B.R. Mottelson, Benjamin, New York, Vol. II, (1975)
[20] P. Moller, et al., At. Data Nucl. Data Tables 109–110, p. 1 (2016)
[21] J.P. Delaroche et al., Phys. Rev. C 81, p. 014303 (2010)
[22] M. Wang et al., Chin. Phys. C 41, p. 030003 (2017)
[23] J. Erler et al., Nature 486, p. 509 (2012)
[24] W. Noertershaeuser et al., Phys. Rev. Lett. 102, p. 062503 (2009)
[25] B.A. Marsh et al., Nature Physics 14, p. 1163 (2018)
[26] X.F. Yang et al., Phys. Rev. Lett. 116, p. 182502 (2016)
[27] C. Gorges et al., Phys. Rev. Lett. 122, p. 192502 (2019)
[28] P.M. Goddard et al., Phys. Rev. Lett. 110, p. 032503 (2013)
[29] I. Angeli et al., Atom. Data. Nucl. Data Tables 99, p. 69 (2013)